Available online at www.sciencedirect.com
SCIENCE DIRECT®
Journal of Hydrology 281 (2003) 159–171
Journal of Hydrology
www.elsevier.com/locate/jhydrol

Theoretical and experimental studies of coupled seepage-pipe flow to a horizontal well

Chongxi Chen[a], Junwei Wan[a], Hongbin Zhan[b,*]

[a]*Environmental Geology Institute, China University of Geosciences (Wuhan), Wuhan, Hubei 430074, People's Republic of China*
[b]*Department of Geology and Geophysics, Texas A and M University, College Station, TX 77843-3115, USA*

Accepted 22 April 2003

Abstract

This study proposes a new approach, which describes a finite-diameter horizontal well and flow inside the pumping well jointly. This approach utilizes a new treatment for in-well hydraulics, thus eliminating the flux- or head-based boundary condition along the horizontal well. An 'equivalent hydraulic conductivity' concept is applied for treating the horizontal wellbore. This conceptual model is more general than previous models that describe the horizontal wellbore. The description of in-well hydraulics depends on the Reynolds number. A sample case of horizontal well pumping underneath a river is first used to illustrate the solution of the proposed approach. A physical laboratory model was constructed and hydraulic heads and the well flow rate were carefully monitored and compared with the numerically calculated results using the proposed model. The experimental data agree well with the numerical solution.

Keywords: Horizontal well; Pipe flow; Reynolds number; Experiment; Conceptual model; Polygon finite difference method

1. Introduction

Horizontal wells recently generated great interest among hydrogeologists and environmental engineers because of numerous advantages over vertical wells in many hydrological and environmental applications. Studies of flow to horizontal wells in hydrological sciences can be dated back to Hantush and Papadopulos (1962), who investigated flow to a collector well consisting of a series of horizontal wells. Various investigators have conducted studies of ground water flow to horizontal wells in the last decade (Cleveland, 1994; Murdoch, 1994; Falta, 1995; Sawyer and Lieuallen-Dulam, 1998; Zhan, 1999; Hunt and Massmann, 2000; Zhan and Cao, 2000). Petroleum engineers have also done extensive work on horizontal well problems (Goode and Thambynayagam, 1987; Daviau et al., 1988; Ozkan et al., 1989; Rosa and Carvalho, 1989). Kawecki (2000) applied some equations derived in petroleum engineering for use in hydrological problems. Zhan et al. (2001) and Zhan and Zlotnik (2002) have investigated drawdowns generated by pumping horizontal wells in confining aquifers and water table aquifers, respectively. Zhan and Park (2002) provided a study of gas flow to a horizontal well. All the studies mentioned above use

* Corresponding author. Tel.: +1-979-862-7961; fax: +1-979-845-6162.
E-mail address: zhan@hydrog.tamu.edu (H. Zhan).

0022-1694/03/$ - see front matter © 2003 Elsevier B.V. All rights reserved.
doi:10.1016/S0022-1694(03)00207-5

line sinks/sources to simulate horizontal wells, and the finite diameter of the wellbore and in-well flow are not considered. Furthermore, these studies use either a uniform-flux or a uniform-head boundary to treat a horizontal well.

When the screen length of a horizontal well is large, which is often the case, and the flow rate inside the wellbore is not small, head losses inside the horizontal well can be significant and cannot be neglected. Tarshish (1992) recognized the importance of in-well hydraulics and incorporated that type of flow in his numerical simulation. His study was limited by an infinitely long well and steady-state conditions. Furthermore, he considered a special case of flow inside the well, in which the head loss was proportional to the square of the average flow velocity inside the well that implied that the Reynolds number was greater than 100,000 (Olson and Wright, 1990; Munson et al., 1998).

In reality, there are five possible flow regimes inside the wellbore. That is: the hydraulic head loss inside the wellbore can be proportional to velocity u for the laminar regime, to $u^{1.75}$ for the smooth turbulent regime, and to u^2 for the rough turbulent regime. Transitional regimes exist between the laminar regime and the smooth turbulent regime, and between the smooth turbulent regime and the rough turbulent regime (Olson and Wright, 1990; Munson et al., 1998). An adequate model should consider all these possible flow regimes inside the horizontal well in addition to the seepage flow in the aquifer.

Results of several investigations with coupling of seepage flows in aquifers, pipes, and karst channels are currently available. Chen et al. (1993) used the coupled model of seepage-pipe flow to study groundwater flow to wells in multilayer aquifers. This study considered the broad range of head losses and flow velocity inside the conductive pipe, and was used to simulate pumping tests at the Dragon Pool field site (Beihai City, Guangxi Autonomous District of China). Chen (1995) developed a mathematical model of groundwater flow in a karst channel-fracture-porous medium system, and Cheng and Chen (1998) applied this model to a field experiment conducted at a Beishan mining site (Guangxi Autonomous District of China). Chen and Lin (1998) applied this model for another study at the bank of the Yellow River near Zhengzhou City, Henan Province of China. Examples of coupling of groundwater flow with in-well hydraulics for vertical wells were presented by Zlotnik and McGuire (1998a,b), Dinwiddie et al. (1999), Therrien and Sudicky (2001), Zurbuchen et al. (2002), and Zlotnik and Zurbuchen (2003, this issue).

The concept of seepage-pipe flow has not yet been applied to groundwater flow in a horizontal well. The purpose of the present study is to consider the realistic flow regime inside the wellbore that can be laminar, transitional, and turbulent. The line sink/source, uniform-flux, and uniform-head assumptions will not be used. A laboratory experiment is used to test the conceptual model by simulating a horizontal well pumping underneath a river.

2. Flow to a finite-diameter horizontal well

2.1. In-well hydraulics

In a finite-diameter well, there is always hydraulic head loss along the flow path; thus the wellbore cannot be a uniform-head boundary. With a uniform-flux boundary assumption, the head distribution along the wellbore varies and the lowest head is at the center of the wellbore length. This contradicts the fact that the lowest head inside the well is always at the point where water is pumped (wellhead). These assumptions of uniform-flux or uniform-head distribution simplify analytical modeling, but do not reflect the flow processes accurately. When well, aquifer, and seepage through the screen are considered as an integrated flow system, it is easy to define a consistent model without invoking any assumptions about the boundary condition at the horizontal wellbore.

If the hydraulic head at the horizontal wellhead is given, then the following condition is applied

$$H(x = x_{\text{wout}}, y = y_{\text{w}}, z = z_{\text{w}}) = H_{\text{wout}}, \tag{1}$$

where x, y, and z are the Cartesian coordinates; x_{wout} is the x-coordinate of the wellhead; y_{w} and z_{w} are the y and z coordinates of the horizontal wellbore, respectively; H_{wout} is the hydraulic head at the wellhead.

If the pumping rate of the well is known, then the following condition is applied

$$Q(x = x_{\text{wout}}, y = y_{\text{w}}, z = z_{\text{w}}) = Q_{\text{wout}}, \tag{2}$$

where Q_{wout} is the pumping rate of the horizontal well.

Head losses along the cylindrical pipe follow the Darcy–Weisbach equation (Munson et al., 1998; Olson and Wright, 1990)

$$\Delta H = f\frac{l}{d}\frac{u^2}{2g}, \tag{3}$$

where ΔH is the loss of hydraulic head, f is the coefficient of friction or so-called Darcy–Weisbach coefficient, l is the length of water flow, d is the diameter of the pipe, u is the average water flow velocity inside the pipe, and g is the gravity acceleration. The Reynolds number, R_e, is defined as

$$R_e = ud/\nu, \tag{4}$$

and ν is the kinematic viscosity.

The coefficient f is a function of the Reynolds number and the relative roughness of the inner wall of the well (e/d), where e is a measure of the roughness of the pipe wall

$$f = \phi(R_e, e/d). \tag{5}$$

For certain ranges of the Reynolds number, the following formulae are found valid. When $R_e < 2300$, flow inside the well is laminar, and the coefficient of friction is $f = 64/R_e$. When $R_e > 100,000$, f becomes independent of the Reynolds number R_e; rather, it only depends on the relative roughness of the inside wall of the pipe (Munson et al., 1998). This range of the Reynolds number is called the rough turbulent region, in which the hydraulic head loss ΔH is proportional to u^2:$\Delta H \propto u^2$. When $3000 < R_e < 100,000$, there exists a relationship $f = 0.316/R_e^{0.25}$, called the smooth turbulent region, in which $\Delta H \propto u^{1.75}$ (Munson et al., 1998).

The focus of this study is to couple the groundwater flow outside the well with the flow inside the well. In order to solve this problem, the concept of an equivalent porous medium is proposed. The specific discharge along the well is $q = u(x,t)$. Eq. (3) can be rewritten in Darcian form for in-well flow as follows

$$q = (2gd/fq)J, \tag{6}$$

where $J = -\Delta H/l$ is the negative gradient of flow inside the well. The equivalent hydraulic conductivity under the non-seepage pipe flow condition, denoted as K_{n}, is defined as

$$K_{\text{n}} = 2gd/fq. \tag{7}$$

Equivalent porosity of in-well flow equals unity. The specific discharge inside the well follows the 'apparent' form of Darcy's Law, and the in-well pipe flow and groundwater flow are integrated into a unified form.

2.2. Coupled model

The mathematical model of groundwater flow to a horizontal well is as follows

$$\begin{aligned}
&\frac{\partial}{\partial x}\left(K_{\text{e}}\frac{\partial H}{\partial x}\right) + \frac{\partial}{\partial y}\left(K_{\text{e}}\frac{\partial H}{\partial y}\right) + \frac{\partial}{\partial z}\left(K_{\text{e}}\frac{\partial H}{\partial z}\right) + \varepsilon \\
&\quad = S_{\text{s}}\frac{\partial H}{\partial t}, \quad (x, y, z \in D,\ 0 < t \le t_e) \\
&H(x, y, z, t)|_{t=0} = H_0(x, y, z), \quad (x, y, z \in D) \\
&H(x, y, z, t)|_{B1} = H_1(x, y, z, t), \quad (0 < t \le t_e) \\
&\frac{\partial H}{\partial n}(x, y, z, t)|_{B2} = V(x, y, z, t), \quad (0 < t \le t_e) \\
&H(x_{\text{wout}}, y_w, z_w, t) = H_{\text{wout}}(t), \quad \text{or} \quad (0 < t \le t_e) \\
&Q(x_{\text{wout}}, y_w, z_w, t) = Q_{\text{wout}}(t), \quad (0 < t \le t_e)
\end{aligned} \tag{8}$$

$$K_e = \begin{cases} K, & \text{hydraulic conductivity of the aquifer} \\ K_{\text{l}}, & \text{equivalent hydraulic conductivity of laminar flow inside the well} \\ K_{\text{n}}, & \text{equivalent hydraulic conductivity of turbulent flow inside the well,} \end{cases}$$

where K_{e} is the equivalent hydraulic conductivity including both aquifer and wellbore; S_{s} is the specific storage; H is the hydraulic head; ε is the source term;

H_0 is the initial hydraulic head; H_1 is the first type boundary condition; V is the water flux rate per unit area for the second type boundary condition; B_1 and B_2 represent the first- and second- type boundary conditions, respectively; n is the outward normal direction; D is the study domain; and t_e is the study period. The usage of the first- and second-type boundary conditions implies that this model works with confining aquifers and with aquifers underneath rivers or lakes, but does not work with water table aquifers. This mathematical model can be extended to handle a water table aquifer by including the following boundary condition at elevation z_{wt} at the water table (Neuman, 1974)

$$K_z \frac{\partial h(x,y,z_{wt},t)}{\partial z} + S_y \frac{\partial h(x,y,z_{wt},t)}{\partial t} = 0, \quad (9)$$

where S_y is the specific yield. Additional discussion of different water table aquifer models can be found in Moench (1995).

Rigorously speaking, one should consider additional well loss due to radial flow through the slots of the well screen. Such distributed radial inflow generates extra energy loss as follows: the radial flow direction changes to axial at the inside wall of the pipe, the above flow conversion processes at the wall reduce the cross section occupied by pure axial flow inside the pipe, and water particles carried by radial inflow should accelerate from zero to the average axial flow velocity. The mathematical modeling of incorporating radial flow well loss with the Darcian flow in the aquifer and the pipe flow inside the well is challenging. Most of the vertical-well studies on coupled Darcian-pipe flow systems do not consider the radial flow well-loss (Zlotnik and McGuire, 1998a,b; Dinwiddie et al., 1999; Therrien and Sudicky, 2001; Zlotnik and Zurbuchen, 2003, this issue). In general, the pumping rate of a horizontal well is distributed over a long screen, thus the pumping rate per unit length of screen of a horizontal well is often relatively small. Therefore, the radial flow to the horizontal well often has a slow velocity, resulting in less significant radial flow well-loss. Nevertheless, it is interesting to investigate the problem of coupling both well losses across the well screen and inside the well-bore with the aquifer Darcian flow. This task is beyond the scope of this article and will be studied in the future.

3. A numerical example: horizontal well underneath a river

We will show that in general uniform-flux or uniform-head boundary condition is not valid at the horizontal well screen, and that the errors associated with using the uniform-flux or uniform-head conditions could be significant. The model proposed in this study can be used to determine when the uniform-head and uniform-flux conditions are valid. The Polygon Finite Difference (PFD) method will be used to solve the problem in this study (Narasimhan and Witherspoon, 1976). Although this problem can also be solved using the standard Finite Difference method that uses rectangular grid blocks, the PFD method is preferred when the boundaries of the aquifers are irregular, the geometrical shapes of the heterogeneous zones are irregular, and the locations of the wells are irregular. The PFD method has been previously investigated by various authors (Fowler and Valentine, 1963; Chun et al., 1963; Tyson and Weber, 1964; Thomas, 1973; Narasimhan and Witherspoon, 1976; Chen and Pei, 2001).

Fig. 1 shows the layout of a horizontal well pumping underneath a river. The following parameters are used. The length, width, and thickness of the aquifer are $l = 116$ m, $w = 3777.4$ m, and $b = 13.8$ m, respectively. The aquifer is homogeneous and isotropic with hydraulic conductivity $K = 1.0$ m/day. The specific storage is $S_s = 10^{-5}$ m^{-1}. The horizontal well is at the center of the aquifer and its length equals l. The well diameter is 0.05 m. The lateral and bottom boundaries of the aquifer are no-flow boundaries

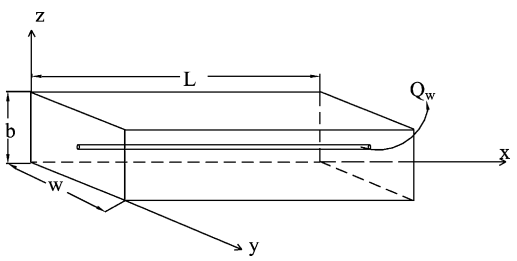

Fig. 1. Layout of the simulation domain.

and the upper boundary is a constant head boundary: $H_1 = 10$ m. The initial head is 10 m throughout the aquifer. The wellhead at the right end of the horizontal well has the first type boundary condition where the head decreases at a rate of 10 m/day. The decreasing head at the wellhead simulates the drawdown caused by the pumping. The dynamics of flow to the horizontal well will be simulated for 1.0 day with time step sizes starting from a few seconds to 10 min at the end of simulation.

Thirty evenly distributed grid points are assigned along the length of the horizontal well (grid step 4.0 m). Twenty-five unevenly distributed grid points with grid steps between 0.2 and 1000 m are assigned along the width of the aquifer, and 15 unevenly distributed grid points with grid steps between 0.2 and 2.0 m are assigned along the depth of the aquifer. Large grid steps at large distances from the horizontal well are selected in order to simulate the lateral boundary at infinity.

Three grid points on the same plane make a triangle that is used to construct the hexagonal grid block. The finest grid steps are used at places closest to the horizontal well, and progressively greater grid steps are used at larger distances from the well. There are a total 11,250 grid points.

Fig. 2 shows the drawdown distribution along the axis of the horizontal well at $t = 1.0$ day. The drawdown increases from 3.58 m at the first grid point (the left end of the well) in Fig. 2 to 10.0 m at the 30th grid point, which is the wellhead (the right end of the well). The latter is 2.8 times more than the former. Therefore, it is inadequate to use a uniform-head boundary condition to describe the horizontal well. The flux rate at the wellhead increases from 10.9 m^3/d at $t = 0.01$ day to 574.6 m^3/d at end of the simulation $t = 1.0$ day.

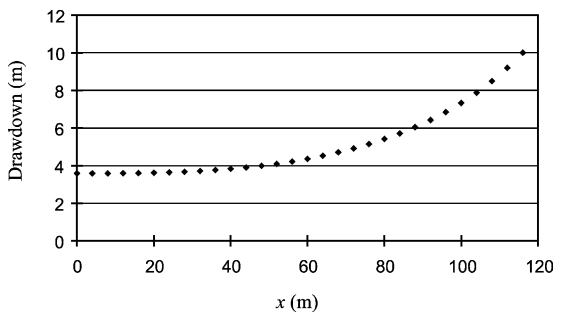

Fig. 2. The drawdown distribution along the axis of the horizontal well at the end of the simulation $t = 1.0$ day.

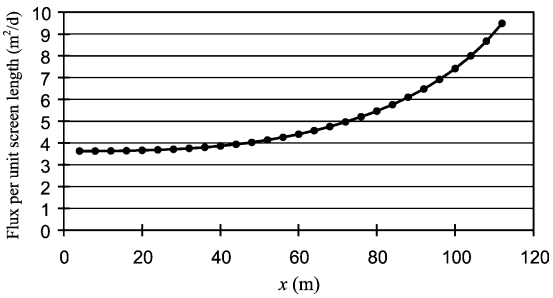

Fig. 3. The water flux per unit length along the axis of the horizontal well at the end of the simulation $t = 1.0$ day.

Fig. 3 shows the water flux distribution along the axis of the well at $t = 1.0$ day. The water flux per unit length along the axis of the horizontal well increases from 3.63 m^2/d at the first segment (left end of the well) to 9.50 m^2/d at the 29th segment (right end of the well) at $t = 1.0$ day. The latter is 2.6 times more than the former. Furthermore, this ratio changes continuously with time. It is clearly inadequate to use a uniform-flux boundary condition to describe the horizontal well hydraulics.

Most previous approaches do not consider the in-well flow, which depends on the well diameter and the Reynolds number. Fig. 4 shows the distribution of equivalent hydraulic conductivity of the horizontal wellbore at the end of the simulation. We find that

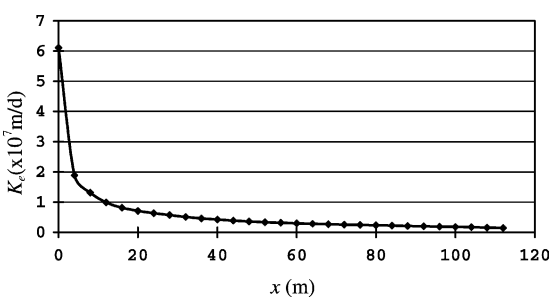

Fig. 4. The equivalent hydraulic conductivity K_e distribution along the axis of the horizontal well at the end of the simulation $t = 1.0$ day.

the equivalent hydraulic conductivity at the first segment (left end of the horizontal well) is 6.11×10^7 m/d. It then decreases rapidly when moving to the right, and eventually reaches 1.46×10^6 m/d at the right end of the well.

4. Laboratory study of flow to a finite-diameter horizontal well

The purpose of the experiment is to test the developed theoretical model and to gain further insights into the horizontal well hydraulics. A sandbox model was used to simulate an aquifer underneath a river. A horizontal pumping well was constructed near the bottom of the sandbox. Fig. 5 illustrates the sandbox model used in the experiment and Fig. 6 shows the experimental design, which includes a rectangular sandbox, a water recharge-discharge system, pressure transducers, a flow meter, and data collecting and analyzing systems.

4.1. Physical model

The rectangular sandbox is 453 cm long in the *x*-direction, 50 cm wide in the *y*-direction, and 120 cm high in the *z*-direction. The origin of the coordinates is at the front-left corner of the bottom plane. The top of the sandbox is open for sand loading and water supplying. In order to reduce sandbox deformation during the experiment, the sandbox is made from 10 mm thick steel on the back and sides, and the front side is made from 5 mm thick transparent steel-reinforced glass for visual observation.

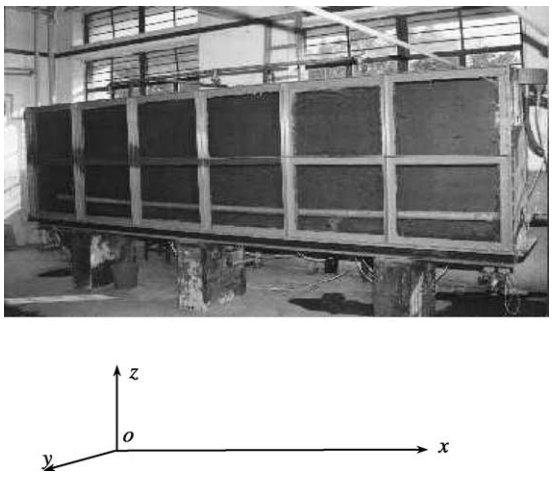

Fig. 5. The sandbox model used in the laboratory experiment. The horizontal well is near the bottom of the sandbox.

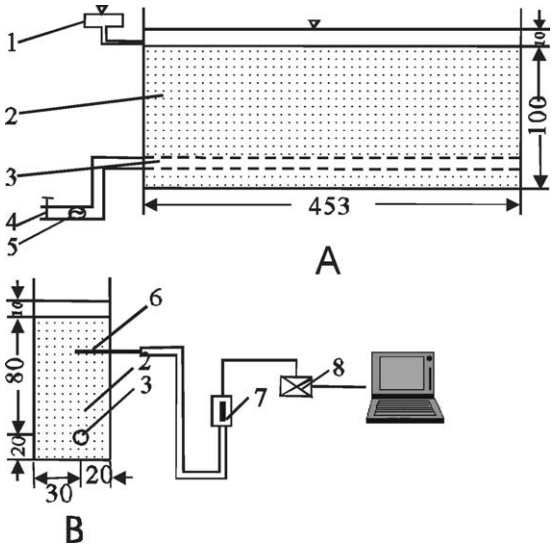

Fig. 6. Experiment design: (A) the *xz*-cross section of the sandbox, (B) the *yz*-cross section of the sandbox. (1) Water tank for maintaining a 10 cm thick water layer above the sand; (2) sand load; (3) horizontal well; (4) water valve; (5) electromagnetic flow meter; (6) pressure transducer; (7) pressure gauge; (8) AD converter and (9) computer.

The four lateral vertical planes and the bottom plane of the sandbox are no-flow boundaries. The top boundary is chosen as a known head boundary. This boundary is the major water source during the pumping period. In addition, water exits are installed at both sides of the sandbox (Fig. 6) to make sure that the water layer at the top always remains about 10 cm thick (a 'river'). Such a water layer will ensure that the river will not become dry and will also prevent the entrance of air into the aquifer.

There are two considerations when choosing the porous medium in this experiment. In order to ensure Darcy's law applicability, the sand grains should not be too coarse. In order to ensure that laminar and turbulent flow regimes exist inside the horizontal well, a high flow rate is needed; thus, the sand should not be too fine. Based on these considerations, medium coarse sand with grain diameter

between 0.25 and 1.0 mm was chosen. This sand was water-washed, and then packed in the sandbox. During the sand packing process, the specific weight of the sand is controlled to ensure that the sand is homogeneous and isotropic. The total thickness of the sand inside the box is 100 cm.

In order to have various flow regimes inside the horizontal well, a large sandbox and highly permeable sand are needed. The horizontal well should be installed near the bottom of the sandbox to maintain a sufficiently large hydraulic head difference between the horizontal well and the river. In this experiment, a horizontal well with an inner diameter of 5.42 cm is set at a location 20.0 cm above the bottom plane ($z = 20$ cm) and 20.0 cm from the front plane ($y = 20.0$ cm) inside the sandbox. The outer diameter of the horizontal well is 6.0 cm and the length of the well screen equals the length of the sandbox. Simplified calculations using uniform-head for horizontal well indicate that both the laminar and turbulent regimes will occur inside the well. The screen of the horizontal well is made from PVC pipe with a 5.0 mm space between the 1.0 mm open slots. A thin geotextile net is wrapped around the screen to prevent well clogging. The horizontal well was deliberately shifted from the symmetry plane ($y = 25.0$ cm) to $y = 20.0$ cm in order to gain more information about the three-dimensionality of the flow.

Ten pressure transducers were used in the experiment. Eight of them were uniformly distributed at different locations at different depths. The coordinates of these eight pressure transducers are shown in Table 1. One of the remaining two is installed in the river above the sand layer to record the change of the water level in the river, and the other is installed at the exit of the horizontal well, which is outside the sandbox and is 31.0 cm away from the closest inner wall of the sandbox (Fig. 7). An electromagnetic flow meter was installed at the wellhead to record the change of flow rate. A valve was used to control the flow rate of the well.

Table 1
Locations of the pressure transducers

Transducer number	x (cm)	y (cm)	z (cm)
1	41.5	20	80
2	41.5	20	10
3	156.5	30	60
4	226.5	20	40
5	226.5	20	10
6	296.5	30	60
7	401.5	20	80
8	401.5	20	10

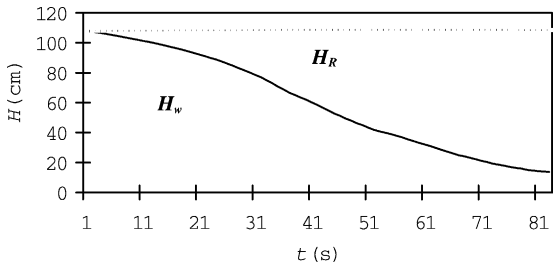

Fig. 7. The water level of the 'river' above the sand level (H_R) and the hydraulic head at the exit of the horizontal well (H_w) as functions of time.

An AD converter was used to digitize the electric signals from the pressure transducers and flow meter, which were recorded and analyzed by an on-site computer that displayed the data output graphically on the screen. Data acquisition frequency for the pressure transducers and flow meter was 1 Hz.

4.2. Experimental procedures

After setting up all the required instruments, the sand was saturated by opening the water intake at the sandbox bottom and slowly saturating the sand from the bottom to the top. The employed 24 h water saturation process minimized the presence of air bubbles in the sand. During the experiment, the water intake at the sandbox bottom was shut off, and water was supplied to the top of the sandbox. After several minutes of waiting to ensure that the head inside the sand is at steady-state, the valve of the horizontal well water exit was opened. At the same time, the hydraulic heads and flow rate were recorded, and the results were shown on the computer screen. The valve was gradually opened to increase the flow rate of the horizontal well to its maximum, and then the flow rate stabilized for several seconds. The experiment was completed after closing the valve.

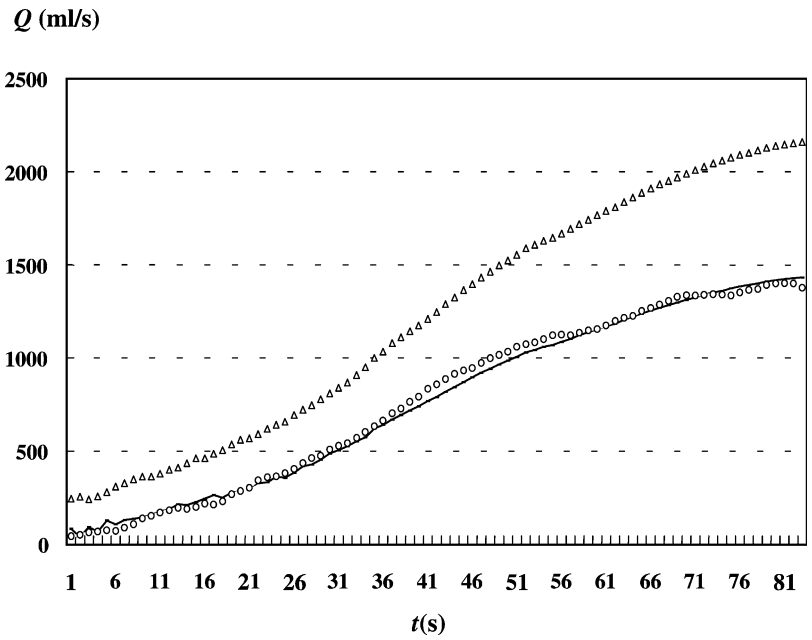

Fig. 8. The flow rate at the exit of the horizontal well. The circles in the diagram are the measured values. Modeling results (solid line) were calculated using different vertical hydraulic conductivity for the top layer (layer 11) and the rest layers (layer 1–10). The triangles present the modeling results using a uniform vertical hydraulic conductivity.

4.3. Experimental results and comparison with the theory

In the experiment, the flow rate in the horizontal well starts at 0.0 cm^3/s and gradually increases to 1403 cm^3/s within 83 s. The water level in the river, denoted as H_R, and the hydraulic head at the wellhead, denoted as H_w, are plotted against time in Fig. 7. The corresponding flow rate in the horizontal well versus time is plotted in Fig. 8, and hydraulic heads at the piezometers inside the sandbox are plotted in Fig. 9.

These results are compared with the results of numerical modeling. In the numerical model of the sandbox, 46 grid points were located along the x-axis, and 11 uniform grid points (grid step 5.0 cm) were located along the y-axis, and 11 grid points (grid step 10.0 cm) were located along the z-axis. An additional grid point was added at the exit of the horizontal well. Thus the total number of grid points were $46 \times 11 \times 11 \times 1 = 5567$. The PFD method was applied.

The hydraulic conductivity and specific storage of the sandbox and the friction coefficient for the horizontal well pipe are needed for the numerical model. The hydraulic conductivity and specific storage were obtained by inverse modeling, which included fitting the calculated hydraulic heads to the measured piezometer heads. Initial estimations of these parameters were obtained as follows. A falling head permeameter test yielded hydraulic conductivity of the sand $K = 0.136$ cm/s. Considering the fact that the sand packing was relatively homogeneous and isotropic, $K = 0.136$ cm/s was used as the initial estimate for horizontal and vertical hydraulic conductivity values. The initial specific storage was $S_s = 10^{-5}\ cm^{-1}$ using data from similar sediments (Domenico and Schwartz, 1998). Study of the friction coefficient in a pipe is quite standard in fluid mechanics (Munson et al., 1998; Olson and Wright, 1990). The inner roughness of the PVC pipe was estimated as $\Delta = 0.002$ mm. Using well diameter $d = 54.2$ mm, the friction coefficient was obtained using the Moody diagram (Moody, 1944).

Fig. 8 shows the comparison of experimental data with the numerical modeling results. The following parameters are obtained. The horizontal hydraulic conductivity is found to be $K_h = 0.124$ cm/s; the vertical hydraulic conductivity of layers 1–10 is

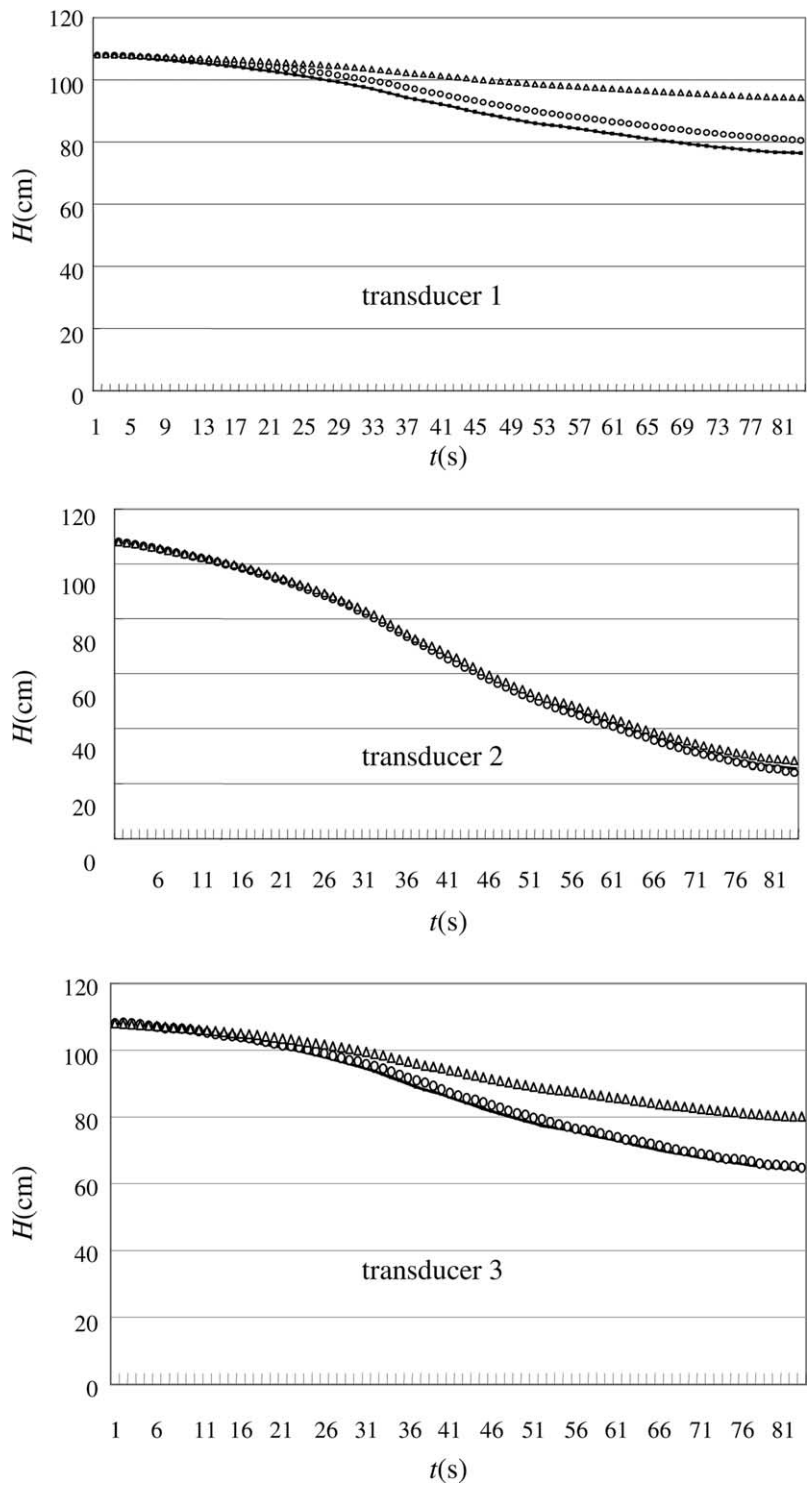

Fig. 9. The observed and simulated hydraulic heads in various transducers. The circles represent the measured values. Modeling results (solid line) were calculated using different vertical hydraulic conductivity for the top layer (layer 11) and the rest layers (layer 1–10). The triangles present the modeling results using a uniform vertical hydraulic conductivity. The locations of the pressure transducers are given in Table 1.

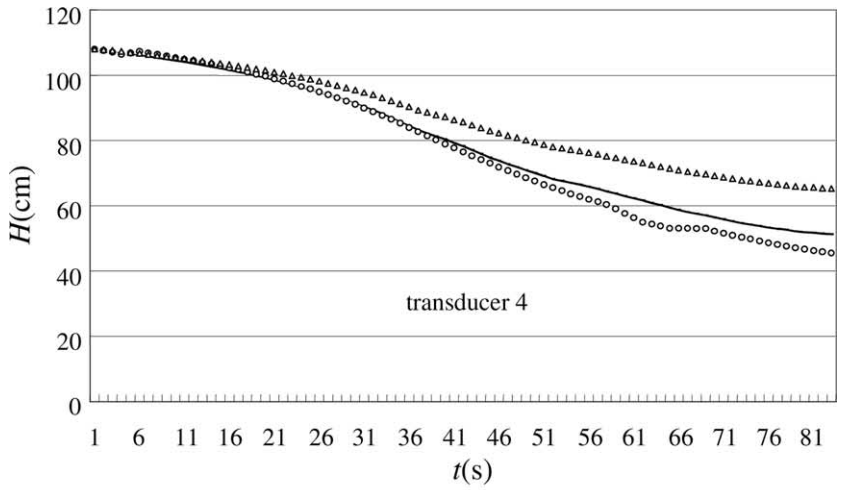

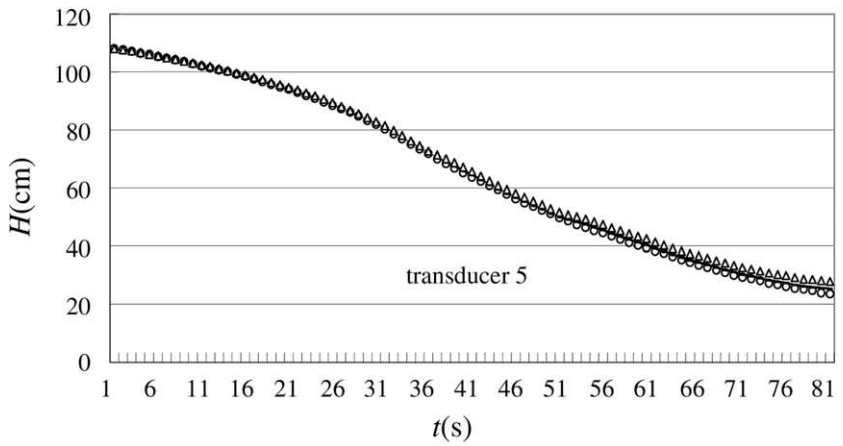

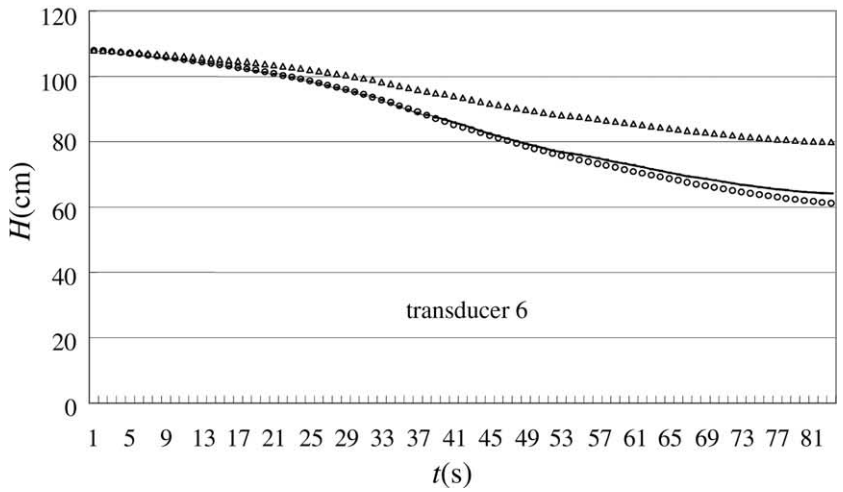

Fig. 9 (*continued*)

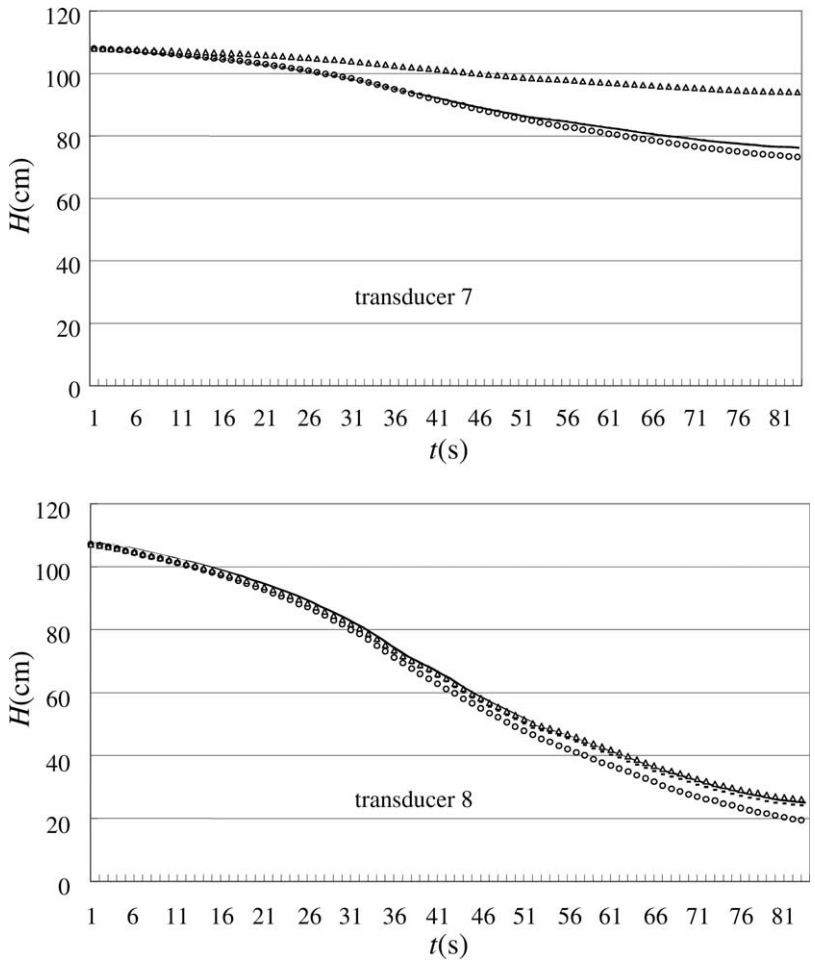

Fig. 9 (*continued*)

$K_z = 0.124$ cm/s, where the layer number increases along the z-axis; the vertical hydraulic conductivity of layer 11 (the top layer) is $K_z = 0.0127$ cm/s; and the specific storage for all layers is $S_s = 1.13 \times 10^{-4} \times$ cm^{-1}. Figs. 8 and 9 show that the flow rate from the horizontal well and the hydraulic heads at all the observation points fit well with the measured data.

At the initial stage of the model simulation, a uniform vertical hydraulic conductivity was assumed that did not yield a good fit. In addition, the calculated flow rates at the exit of the horizontal well were much larger than the measured ones. When a smaller vertical hydraulic conductivity was used to simulate the very top layer (layer 11), a better fit with the experiment was achieved. There are several possible reasons for this. The process of loading and packing sand into the sandbox could accumulate finer sands at the top. The second reason is that the air bubbles were not entirely removed from the top layer, thus reducing hydraulic conductivity because of the presence of air.

The flow rate in the well, Q, (less than 98.8 cm^3/s) corresponds to a Reynolds number along the horizontal well of less than 2300, which corresponds to the laminar flow regime. However, when Q gradually increases to its maximum (1403 cm^3/s), the Reynolds numbers along the horizontal well increased gradually. The laminar flow appears between grid points 1–2, the laminar-smooth turbulent transitional flow appears between grid points 3–4, the smooth turbulent flow appears between grid points 5–18,

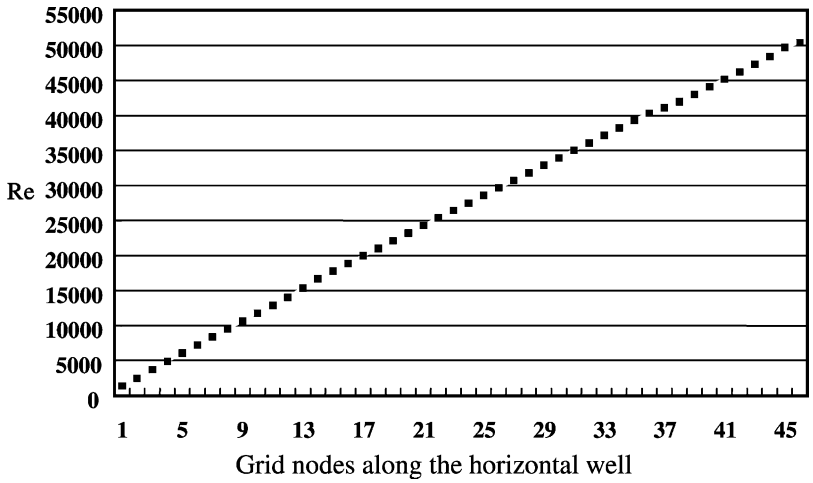

Fig. 10. The Reynolds number distribution along the horizontal well at the end of the experiment (the grid point 1 is the farthest from the wellhead and the grid point 45 is the closest to the wellhead.

and the smooth turbulent-rough turbulent transitional flow appears between grid points 19–45 (Fig. 10). By increasing the length of the horizontal well above 4.53 m, it will be possible to create five different flow regimes inside the well.

5. Summary

This study provides a coupled model of groundwater flow to a horizontal well without adopting the commonly used assumptions of uniform-flux or uniform-head boundaries or the line sink/source model. It combines the aquifer-horizontal wellbore into a heterogeneous porous medium by assigning an equivalent hydraulic conductivity defined by the flow Reynolds numbers inside the well. Laminar, transitional, and turbulent flow regimes inside the horizontal well were considered.

Using a simplified numerical model of a horizontal well underneath a river, we showed that the use of either a uniform-flux or a uniform-head boundary condition on the well screen misrepresents the realistic flux or head distribution along the horizontal wellbore.

A laboratory experiment compared well with the proposed conceptual model. This experiment included horizontal well pumping underneath a river. The horizontal well diameter was chosen to be large (inner diameter 5.42 cm) to achieve a sufficiently high flow rate that induces laminar, transitional, and turbulent regimes in the well. Hydraulic head near the well and flow rate of the well were measured. The experimental results were compared with results of numerical modeling. We found a good agreement between both results.

Acknowledgements

This research is partly supported by the China National Natural Science Foundation (Grant # 49872081) and US National Science Foundation (Grant #BES-9909964). We sincerely thank Vitaly A. Zlotnik and an anonymous reviewer for their detailed and critical review that helped us to greatly improve the quality of the manuscript. Thank to one of the Editors, Marios A. Sophocleous for his great personal review of the manuscript.

References

Chen, C., 1995. Study of ground water flow model and simulation in three-porosity system of karst channel-fracture-porous medium. J. China Univ. Geosci. (Earth Science) 20 (4), 361–366.in Chinese.

Chen, C., Lin, M., 1998. Groundwater Flow Model of Mixed Well and its Application, Publishing House of China University of Geosciences, Wuhan, China, in Chinese.

Chen, C., Pei, S., 2001. Numerical Simulation of Groundwater Pumping-Subsidence and Prevention Strategy Studies: a Case Study about Suzhou City, Jiangsu Province of China, Publishing House of China University of Geosciences, Wuhan, China, in Chinese.

Chen, C., Jiang, J., Lin, M., 1993. Theory and Application of Model Coupling Seepage-Pipe Flow for Unsteady Multilayer Pumping Tests, Science and Technical Report, No. 88172K051, Environmental Geology Institute, China University of Geosciences (Wuhan), in Chinese.

Cheng, J., Chen, C., 1998. Preliminary numerical study of Karst groundwater flow in Beishan area. Proceeding of Second International Conference of Future Groundwater at Risk, July 13–17, pp. 65–66.

Chun, R.Y.D., Weber, E.M., Mido, K., 1963. Computer tools for sound management of groundwater basins. Int. Assoc. Sci. Hydrol. Berkeley. Publ. No. 64, 427–437.

Cleveland, T.G., 1994. Recovery performance for vertical and horizontal wells using semianalytical simulation. Ground Water 32 (1), 103–107.

Daviau, F., Mouronval, G., Bourdarot, G., Curutchet, P., 1988. Pressure analysis for horizontal-wells. SPE Formation Eval. 3 (4), 716–724.

Dinwiddie, L.C., Foley, N.A., Molz, F.J., 1999. In-well hydraulics of the electromagnetic borehole flowmeter. Ground Water 37 (2), 305–315.

Domenico, P.A., Schwartz, F.W., 1998. Physical and Chemical Hydrogeology, second ed, Wiley, New York.

Falta, R.W., 1995. Analytical solutions for gas-flow due to gas injection and extraction from horizontal-wells. Ground Water 33 (2), 235–246.

Fowler, L.C., Valentine, V.E., 1963. The coordinated use of groundwater basins and surface water delivery facilities. Int. Assoc. Sci. Hydrol. Berkeley. Publ. No. 64, 376–383.

Goode, P.A., Thambynayagam, R.K.M., 1987. Pressure drawdown and buildup analysis of horizontal wells in anisotropic media. SPE Formation Eval. 2 (4), 683–697.

Hantush, M.S., Papadopulos, I.S., 1962. Flow of ground water to collector wells. J. Hydraulics Div., Proc. Am. Soc. Civil Engrs. HY 5, 221–244.

Hunt, B., Massmann, J.W., 2000. Vapor flow to trench in leaky aquifer. J. Envir. Engr. 126 (4), 375–380.

Kawecki, M.W., 2000. Transient flow to a horizontal water well. Ground Water 38 (6), 842–850.

Moench, A.F., 1995. Combining the Neuman and Boulton models for flow to a well in an unconfined aquifer. Ground Water 33 (3), 378–384.

Moody, L.F., 1944. Friction factors for pipe flow. Trans. ASME 66 (8), 671–684.

Munson, B.R., Young, D.F., Okiishi, T.H., 1998. Fundamentals of Fluid Mechanics, third ed, Wiley, New York, USA.

Murdoch, L.C., 1994. Transient analyses of an interceptor trench. Water Resour. Res. 30 (11), 3023–3031.

Narasimhan, T.N., Witherspoon, P.A., 1976. An integrated finite difference method for analyzing fluid flow in porous media. Water Resour. Res. 12 (1), 57–64.

Neuman, S.P., 1974. Effect of partial penetration on flow in unconfined aquifers considering delayed gravity response. Water Resour. Res. 10 (2), 303–312.

Olson, R.M., Wright, S.J., 1990. Essentials of Engineering Fluid Mechanics, fifth ed, Harper and Row Publishers, New York, USA.

Ozkan, E., Raghavan, R., Joshi, S.D., 1989. Horizontal-well pressure analysis. SPE Formation Eval. 4 (4), 567–575.

Rosa, A.J., Carvalho, R.de. S., 1989. A mathematical model for pressure evaluation in an infinite-conductivity horizontal well. SPE Formation Eval. 4 (4), 559–566.

Sawyer, C.S., Lieuallen-Dulam, K.K., 1998. Productivity comparison of horizontal and vertical ground water remediation well scenarios. Ground Water 36 (1), 98–103.

Tarshish, M., 1992. Combined mathematical model of flow in an aquifer-horizontal well system. Ground Water 30 (6), 931–935.

Therrien, R., Sudicky, E.A., 2001. Well bore boundary conditions for variably saturated flow modeling. Adv. Water Resour. 24, 195–201.

Thomas, R.G., 1973. Groundwater models. Irrigation and Drainage Paper 21, Food and Agricultural Organisation of the UN, Rome, 192pp.

Tyson, H.N., Weber, E.M., 1964. Ground water management for the nation's future-computer simulation of ground-water basins. J. Hydraulics Div., Proc. Am. Soc. Civil Engrs. HY 4, 59–77.

Zhan, H., 1999. Analytical study of capture time to a horizontal well. J. Hydrol. 217, 46–54.

Zhan, H., Cao, J., 2000. Analytical and semi-analytical solutions of horizontal well capture times under no-flow and constant-head boundaries. Adv. Water Resour. 23 (8), 835–848.

Zhan, H., Park, E., 2002. Vapor flow to horizontal wells in unsaturated zones. Soil Sci. Soc. Am. J. 66 (3), 710–721.

Zhan, H., Zlotnik, V.A., 2002. Ground water flow to horizontal and slanted wells in water table aquifers. Water Resour. Res. 38 (7) 101029/R000401.

Zhan, H., Wang, L.V., Park, E., 2001. On the horizontal-well pumping tests in anisotropic confined aquifers. J. Hydrol. 252 (1–4), 37–50.

Zlotnik, V.A., McGuire, V.L., 1998a. Multi-level slug tests in highly permeable formations: 1. Modification of the Springer-Gelhar (SG) model. J. Hydrol. 204, 271–282.

Zlotnik, V.A., McGuire, V.L., 1998b. Multi-level slug tests in highly permeable formations: 2. Hydraulic conductivity identification, method verification, and field applications. J. Hydrol. 204, 283–296.

Zlotnik, V.A., Zurbuchen, B.R., 2003. Estimation of hydraulic conductivity from the borehole flowmeter tests considering head losses. J. Hydrol this issue.

Zurbuchen, B.R., Zlotnik, V.A., Butler, J.J. Jr., 2002. Dynamic interpretation of slug tests in highly permeable aquifers. Water Resour. Res. 38 (3) 101029/R000354.